Three-dimensional seismic imaging of a protoridge axis in the Main Ethiopian rift

K. Keranen
S.L. Klemperer
Department of Geophysics, Stanford University, Stanford, California 94305-2215, USA
R. Gloaguen Department of Geology, TU "Bergakademie" Freiberg, B. von Cotta 2, 09599 Freiberg, Germany
EAGLE Working Group*

ABSTRACT

Models of continental breakup remain uncertain because of a lack of knowledge of strain accommodation immediately before breakup. Our new three-dimensional seismic velocity model from the Main Ethiopian rift clearly images mid-crustal intrusions in this active, transitional rift setting, supporting breakup models based on dike intrusion and magma supply. The most striking features of our velocity model are anomalously fast, elongate bodies (velocity, V_p ~6.5–6.8 km/s) extending along the rift axis, interpreted as cooled mafic intrusions. These 20-km-wide and 50-km-long bodies are separated and laterally offset from one another in a right-stepping en echelon pattern, approximately mimicking surface segmentation of Quaternary volcanic centers. Our crustal velocity model, combined with results from geologic studies, indicates that below a depth of ~7 km extension is controlled by magmatic intrusion in a ductile middle to lower crust, whereas normal faulting and dike intrusion in a narrow zone in the center of the rift valley control extension in the brittle upper crust. This zone is inferred to be the protoridge axis for future seafloor spreading.

Keywords: Ethiopia, controlled-source seismology, tomography, rifting, magmatism.

INTRODUCTION

The transition from continental rifting to seafloor spreading is difficult to study because most of the evidence is submarine. The Main Ethiopian rift, situated south of seafloor spreading in the Red Sea (Fig. 1, inset), is an excellent location to study how continental rifts develop into oceanic ridges.

A 2003 controlled-source seismic experiment in the Main Ethiopian rift (part of the EAGLE project [Ethiopia-Afar Geoscientific Lithospheric Experiment]; Maguire et al., 2003) recorded data on ~400 km refraction lines along and across the rift and an ~100-km-diameter two-dimensional array spanning the rift at the intersection of the 400 km profiles (Fig. 1). There were 23 explosive sources that ranged from 50 to 5750 kg, with an average shot size of 1100 kg. Shot spacing was nominally 50 km, with a nominal receiver spacing of 1 km in the ~400 km lines and 2.5 km in the two-dimensional array. Approximately 1000 "Texan" seismographs were used with 4.5 Hz geophones along with ~100 broadband seismometers. Initial results show an upper-crustal velocity of ~6.0 km/s on the basis of a consistent Pg arrival across and within the rift (Maguire et al., 2003). Moho depth decreases from 40 km to 30 km from southwest to northeast across the region of Figure 1 (Keller et al., 2004).

Unlike the adjoining Red Sea and Aden rifts, few geophysical studies have been conducted in the Main Ethiopian rift prior to this project. A previous seismic-refraction profile in Afar in 1972 used just 15 seismographs (Berckhemer et al., 1975) and a three-dimensional gravity analysis (Mahatsente et al., 1999) in the region of our study modeled a short-wavelength positive Bouguer anomaly using a 20-km-wide intrusion. Based on these data and field observations, Ebinger and Casey (2001) proposed the idea of localization of strain away from the border faults into narrow magmatic segments in the rift valley.

Here we present the results of our three-dimensional first-arrival traveltime tomography of the middle to upper crust in the Main Ethiopian rift. We image the roots of the rift-valley

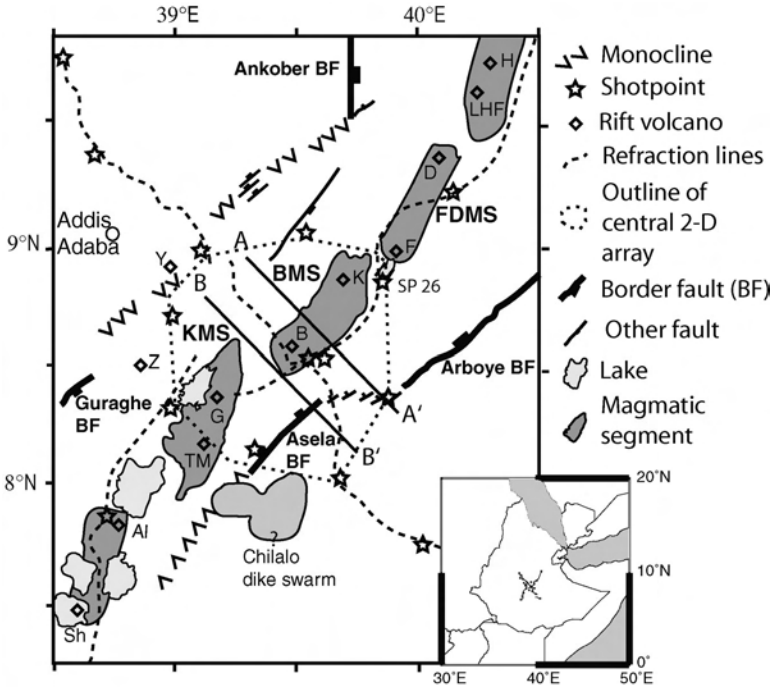

Figure 1. Survey geometry in region of two-dimensional array with respect to magmatic segments and border faults. KMS—Koka magmatic segment, BMS—Boseti magmatic segment, FDMS—Fantale-Dofan magmatic segment; H—Hertale, LHF—Liado Hayk field, D—Dofan, F—Fantale, K—Kone, B—Boseti, Y—Yerer, Z—Zikwala, G—Gademsa, TM—Tullu Moje, Al—Aluto, Sh—Shala. Profiles A–A′ and B–B′ are shown in Figure 3; inset map shows location of our survey in Horn of Africa. Data from shot 26 shown in Fig. DR1 (see text footnote 1). Base map is from Wolfenden et al. (2004).

*EAGLE Working Group includes L. Asfaw, A. Ayele, C. Ebinger, T. Furman, S. Harder, G.R. Keller, G.D. Mackenzie, P.K.H. Maguire, and G.W. Stuart.

volcanoes and crustal modification by magmatism, and we discuss the mode of strain localization in the middle to upper crust.

TECTONIC SETTING

The northeast-trending Main Ethiopian rift cuts across the Ethiopian plateau, which has been interpreted as thermally elevated above at least one mantle plume (Ebinger and Sleep, 1998). Flood basalts from 31 to 29 Ma over a region ~1000 km in diameter are thought to reflect the impact of a plume head beneath the continent (e.g., Pik et al., 1999). Geophysical evidence indicates a deep-seated thermal anomaly consistent with the presence of a plume, with anomalously low P-wave velocities from depths of 650 km beneath Afar (Montelli et al., 2004) to 75 km beneath the Main Ethiopian rift, offset 25 km northwest of the main rift axis (Bastow et al., 2004).

Rift basins in the Main Ethiopian rift are asymmetric, bounded by steep border faults ~50 km long with >3 km throw (Fig. 1; Ebinger and Casey, 2001). Extension began along the border faults by 18 Ma in the southern Main Ethiopian rift, but primary rift development occurred after 11 Ma (WoldeGabriel et al., 1990). Existing geochronology suggests a hiatus in volcanism between 6.5 and 3.2 Ma, when deformation migrated toward a narrow zone in the rift center (Wolfenden et al., 2004). By 1.8 Ma, volcanism and faulting localized to <20-km-wide magmatic segments within the rift (Fig. 1). These magmatic segments include rift volcanoes and young fault belts (Fig. 1), with a north-northeast trend that is oblique to the overall northeast trend of the rift. The segments are separated from one another by ≤20 km in a right-lateral en echelon pattern, and show little correlation with the border faults (Ebinger and Casey, 2001). The extension rate is 8.4 ± 1.4 mm/yr as calculated from plate motions (Horner-Johnson et al., 2003) and 4 mm/yr as measured by the global positioning system (Bilham et al., 1999), 80% of which is concentrated in the magmatic segments. Ebinger and Casey (2001) estimated 35% extension in the rift with as much as 4 km in the upper crust accommodated by dike intrusion during the past 1 m.y. in the ~20-km-wide magmatic segments. Geochemical evidence indicates that the separation of the segments likely persists with depth, as volcanoes within a given segment possess a geochemical signature different from those in neighboring segments (Furman, 2003). Most Quaternary volcanism has occurred in the magmatic segments, beginning ca. 1.6 Ma, but has also occurred off axis at Zikwala and Yerer on the northwest rift shoulder and at Chilalo on the southeast rift shoulder (Fig. 1). Historical flows at Fantale in 1820 (Gibson, 1967) and temperatures of 335 °C at 2.2 km depth in geothermal wells near Aluto (Endeshaw, 1988) indicate ongoing magmatism.

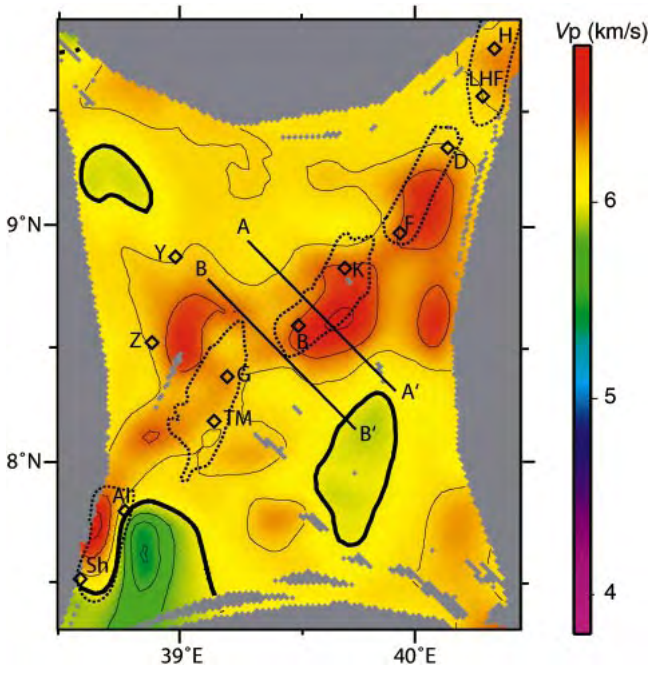

Figure 2. Horizontal slice 10 km depth below rift floor. High-velocity (V_p) bodies below rift axis are interpreted as solidified magmatic intrusions. Lettering, symbols, and area of figure are as in Figure 1; magmatic segments are shown by dotted lines.

TOMOGRAPHY

We used 15 shots in the rift valley and on the rift shoulders to generate 7450 first-arrival traveltime picks for the final inversion. Three-dimensional first-arrival traveltime tomography (Hole, 1992) with a cube of 2 km was used to obtain our velocity model. The final smoothing operator size was 6 × 6 km horizontally × 2 km vertically, and the root mean square error on the final iteration was 117 ms, approximately the picking uncertainty in the data. Examples of data quality and goodness of fit are available in Appendix DR1[1].

Figure 2 shows a horizontal slice 10 km below the rift floor. Elongate, high-velocity bodies (V_p ~6.5–6.8 km/s) are beneath the magmatic segments, with rift volcanoes at each end. These bodies are ~10% faster than the background velocity of 6.0 km/s. The separations between the segments, which are observed at the surface, are visible in our model, particularly between the Koka and Boseti segments. Synthetic tests (Figs. DR2–DR4; see footnote 1) demonstrate that the segmentation is real, not an artifact of poor data coverage. Northwest of the Koka segment, another high-velocity anomaly diverts from the general north-south trend and extends to the northwest, toward the off-axis volcanoes of Zikwala and Yerer (Fig. 1). The Koka segment includes the geothermal prospects of Tullu Moje and Gademsa (Fig. 1) and has slightly slower velocities than the other segments (6.3–6.4 km/s). Although another high-velocity body is present to the east of Kone; it is on the edge of the model and may be an artifact.

A vertical slice across one of the high-velocity bodies is shown in Figure 3A, which extends through the Boseti magmatic segment (A–A′ in Fig. 1). The anomalous body is 20–30 km wide with steep boundaries and rises up to only ~7 km below the rift floor. Also evident is a shallow, low-velocity section (3–5.5 km/s), which is apparently downthrown to the west at the location of the eastern border fault. Beneath this low-velocity layer and away from the high-velocity body, the average velocity in the mid-crust is ~6.0 km/s. Figure 3C shows another slice across the rift valley (B–B′ in Fig. 1) that passes between the surface magmatic segments. No distinct high-velocity body is seen in this slice. The thickness of the low-velocity section is similar in both cross sections.

GEOLOGIC INTERPRETATION

From our velocity model, we interpret that the crust beneath the Main Ethiopian rift is continental, with mainly solidified mafic intrusions beneath the magmatic segments. The average velocity of the mid-crust away from the high-velocity bodies is ~6.0 km/s (Fig. 2), an appropriate value for the Precambrian crystalline basement presumed to underlie the rift. We interpret the distinct high-velocity anomalies beneath the magmatic segments as elongate mafic intrusions into lower-velocity country rock. On the basis of their high seismic velocity in this elevated geothermal regime

[1]GSA Data Repository item 2004155, Appendix DR1 and Figures DR1–DR4, is available online at www.geosociety.org/pubs/ft2004.htm, or on request from editing@geosociety.org or Documents Secretary, GSA, P.O. Box 9140, Boulder, CO 80301-9140, USA.

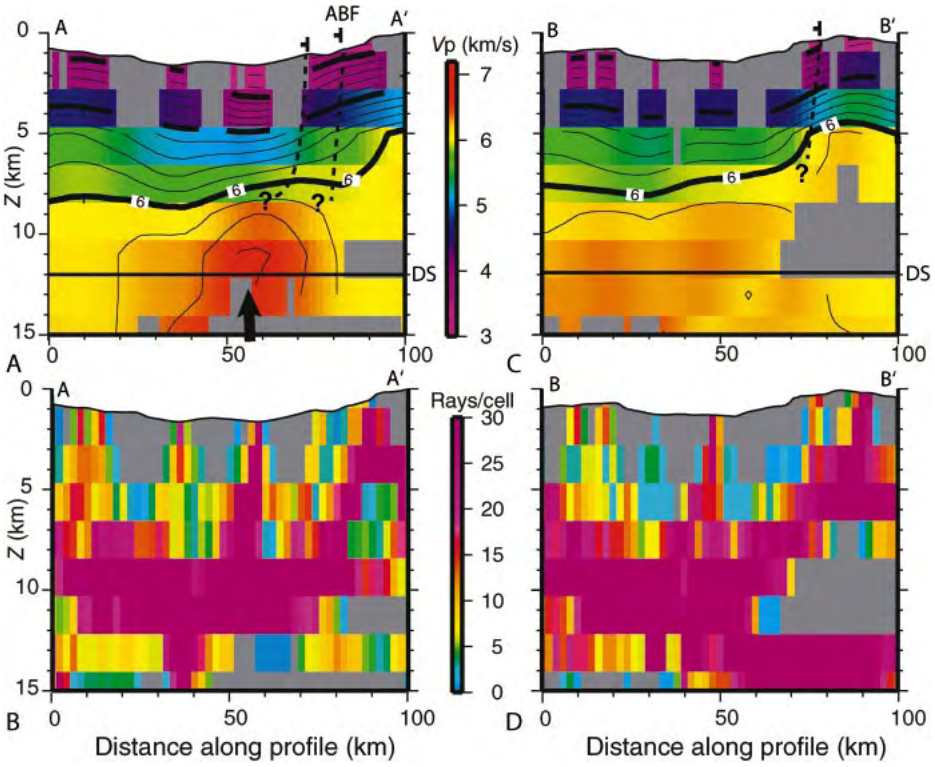

Figure 3. A: Rift-perpendicular cross-section A–A′ extending through Boseti magmatic segment between Boseti and Kone volcanoes (Fig. 1). High-velocity (*Vp*) body (vertical arrow) beneath rift valley is interpreted as solidified mafic magmatic intrusion into Precambrian basement. Faults (⊣ symbols) and proposed subsurface continuation of faults (dashed lines) are marked. Depth of slice (DS) in Figure 2 is marked by horizontal line. Areas with no ray coverage are shown in gray. Vertical exaggeration is 5:1. B: Ray coverage for slice A–A′. C: Rift-perpendicular cross-section B–B′ between magmatic segments (Fig. 1). D: Ray coverage for slice B–B′.

and a modeled density of 3000 kg/m^3 for intrusions in the Main Ethiopian rift (Mahatsente et al., 1999; Keller et al., 2004), the intrusions are almost certainly gabbroic (Christensen and Mooney, 1995). The location of the rift volcanoes at the ends of the magmatic segments differs from the model of Ebinger and Casey (2001), who proposed that central magma chambers feed laterally propagating dikes. Instead, we interpret that the segments, which form as extensional zones perpendicular to the least compressional stress direction (σ_3) of the current stress field (Ebinger and Casey, 2001), behave in the manner of simple cracks. Basaltic magmas move easily through the crust in the center of the segments and erupt from fissures to form flows and cinder cones, but not large calderas. In the complicated stress field near the segment tips, some magma is trapped while rising and undergoes fractional crystallization while assimilating crustal material. The melt that reaches the surfaces from these bodies includes more silicic products that tend to form large calderas.

We interpret the low-velocity section above the intrusions to be primarily flows and ignimbrites deposited over prerift (ca. 26 Ma) flood basalts. These units are exposed in the rift valley (Wolfenden et al., 2004). On the southeastern side of our model, this low-velocity section is offset by what we interpret as the subsurface continuation of the Asela border fault (Fig. 3A, km 80). In Figure 3C the border fault is also imaged, although a magmatic intrusion is not, supporting previous observations that magmatic segments and border faults are not well correlated. An additional fault is interpreted on A–A′ (Fig. 3A, km 60) on the basis of a velocity discontinuity within the low-velocity section, thought to be one of a set of younger faults with unknown offsets masked by young lavas. It is possible that these younger faults sole into the top of the intrusion and continue at a low angle. We note that the estimate of effective elastic thickness in this area is 8 ± 2 km (Ebinger and Hayward, 1996) and that earthquakes are generally shallower than 10 km (Ayele et al., 2004). Mechanisms for low-angle fault development above magmatic injections were presented by Parsons and Thompson (1993). A possibly analogous region is the Colorado River extensional corridor, where an exposed core complex is interpreted to have formed as a massive magmatic intrusion beneath a detachment fault (Campbell-Stone and John, 2003).

Our results show no increase in velocity at shallow depths in the center of the 20-km-wide magmatic segments (Fig. 3A), which indicates that dikes do not constitute a large percentage of the upper-crustal material and have not accommodated the majority of the extension. Synthetic seismic models and calculations of velocity effects due to thin pervasive dike-intrusion models indicate that 30% (i.e., an ~6 km aggregate width) is an approximate upper bound on the degree of dike intrusion, which leaves ~14 km of extension by faulting. The degree of dike intrusion in the last 1 m.y., estimated to be ≤4 km, would not be evident in our data.

TECTONIC INTERPRETATION

Our velocity model lends support to the Ebinger and Casey (2001) model of continental breakup in magmatic provinces that proposes that magmatic segments are the locus of extension in transitional rift settings and that border faults are abandoned prior to continental breakup. We clearly image mafic intrusions ~20 km wide and 50 km long generally located beneath the magmatic segments, which are obliquely oriented with respect to the border faults and accommodate extension in the center of the rift valley. The width of these bodies is compatible with 27 km of extension predicted in the past 3.2 m.y. from plate motions (Horner-Johnson et al., 2003). These separated mid-crustal intrusions may ultimately form the template for a segmented mid-ocean ridge. The orientation and the en echelon geometry of adjacent magmatic segments may be a consequence of the rotation of the least compressional stress direction (σ_3) from northwest-southeast in the late Miocene–Pliocene to west-northwest–east-southeast in the Pleistocene (Wolfenden et al., 2004), in which case the length of the segments would then be controlled by the angle of rotation of the stress field and the width of the rift.

Strain accommodation in the upper crust occurs through a combination of brittle faulting and dike intrusion in the magmatic segments. On the basis of synthetic models, our maximum estimate of mafic material present in the upper crust is 30% of the 20-km-wide dike-bearing segments. This geometry of magmatic intrusions at depth and faulting and dike intrusion in the upper crust (Fig. 4) is similar to that observed beneath slow-spreading mid-ocean ridges such as the Mid-Atlantic Ridge (Sinton and Detrick, 1992). In fact, the very slow separation rate across the Main Ethiopian rift, ~9 mm/yr, would place this rift in the category of ultraslow spreading ridges (Dick et al., 2003), although over the region we studied we did not see the highly attenuated amagmatic accretionary segments that are characteristic of this class of ocean ridge. Although our three-dimensional tomography lacks the aperture to image the lower crust, we speculate that the segmentation continues

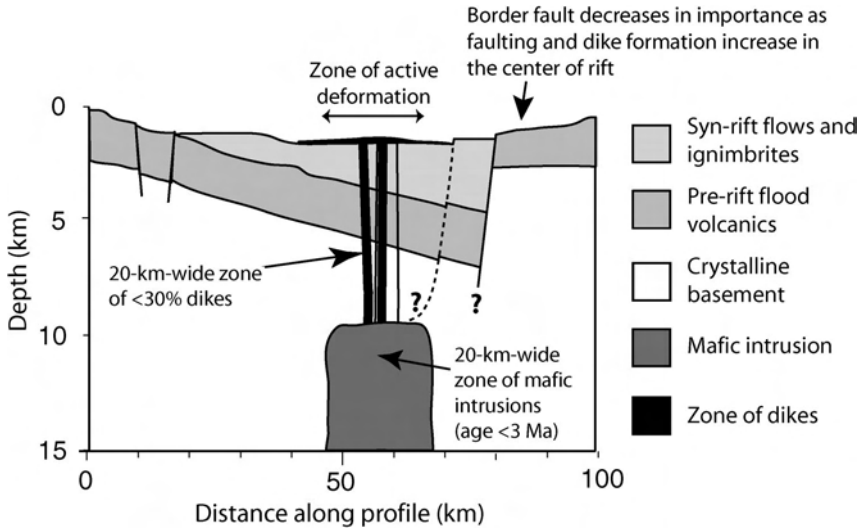

Figure 4. Schematic cross section of upper-crustal structure (along line of Fig. 3A). Mafic intrusion, which continues in elongate zone along rift axis, is interpreted as protoridge axis. Vertical exaggeration is 5:1.

with depth, and presume that it is the more mafic roots of the intrusions we image that will in the future form the high-velocity ''7.x km/s layer'' characteristic of volcanic rifted margins (Menzies et al., 2002).

CONCLUSIONS

Our new seismic velocity model from the Main Ethiopian rift constrains models of continental breakup by imaging massive axial intrusions in a transitional rift environment. Magmatic processes appear to dominate in volcanic rift settings immediately before breakup and control the location of incipient seafloor spreading (cf. Ebinger and Casey, 2001). Above the intrusions, a combination of normal faulting and dike intrusion accommodates extension in the brittle upper crust. These magmatic segments form the protoridge axes for future seafloor spreading and are offset en echelon in the Main Ethiopian rift as a result of oblique rifting.

ACKNOWLEDGMENTS

We thank PASSCAL, SEIS-UK, and DLC for the use of instruments and the entire EAGLE field team. We thank John Hole for the use of his code and Norm Sleep and George Thompson for thoughtful advice. EAGLE data acquisition was funded by National Science Foundation (NSF) Continental Dynamics grant and the Natural Environment Research Council. An NSF graduate fellowship supported K. Keranen.

REFERENCES CITED

Ayele, A., Nyblade, A.A., Langston, C.A., Cara, M., and Leveque, J.-J., 2004, The May 2000 earthquake swarm near Gewane in south Afar, *in* Yirgu, G., et al., eds., Proceedings of International Conference on the East African Rift System, June 20–24 2004, Addis Ababa, Ethiopia: Ethiopian Geoscience and Mineral Engineering Association, p. 23–25.

Bastow, I.D., Stuart, G.W., Kendall, J.-M., Ebinger, C.J., Ayele, A., Cornwell, D.G., and Maguire, P.K.H., 2004, Upper mantle seismic structure of the Northern Ethiopia rift—a region of incipient continental breakup, *in* Yirgu, G., et al., eds., Proceedings of International Conference on the East African Rift System, June 20–24 2004, Addis Ababa, Ethiopia: Ethiopian Geoscience and Mineral Engineering Association, p. 30–33.

Berckhemer, H., Baier, B., Bartelson, H., Behle, A., Burkhardt, H., Gebrande, H., Makris, J., Menzel, H., Miller, H., and Vees, R., 1975, Deep seismic soundings in the Afar region and on the highland of Ethiopia, *in* Pilger, A., and Roesler, A., eds., Afar between continental and oceanic rifting: Stuttgart, Schweizerbart, p. 89–107.

Bilham, R., Bendick, R., Larson, K., Braun, J., Tesfaye, S., Mohr, P., and Asfaw, L., 1999, Secular and tidal strain across the Ethiopian rift: Geophysical Research Letters, v. 27, p. 2789–2984.

Campbell-Stone, E., and John, B., 2003, Temporal changes in deformation mode: From failure to flow in the Colorado River extensional corridor, *in* Klemperer, S.L., and Ernst, G., eds., The lithosphere of western North America and its geophysical characterization: Geological Society of America International Book Series, v. 7, p. 348–363.

Christensen, N.I., and Mooney, W.D., 1995, Seismic velocity structure and composition of the continental crust: A global view: Journal of Geophysical Research, v. 100, p. 9761–9788.

Dick, H.J.B., Lin, J., and Schouten, H., 2003, An ultraslow-spreading class of ocean ridge: Nature, v. 426, p. 405–412.

Ebinger, C.J., and Casey, M., 2001, Continental breakup in magmatic provinces: An Ethiopian example: Geology, v. 29, p. 527–530.

Ebinger, C.J., and Hayward, N., 1996, Soft plates and hot spots: Views from Afar: Journal of Geophysical Research, v. 101, p. 21,859–21,876.

Ebinger, C.J., and Sleep, N.H., 1998, Cenozoic magmatism throughout East Africa resulting from impact of a single plume: Nature, v. 395, p. 788–791.

Endeshaw, A., 1988, Current status (1987) of geothermal exploration in Ethiopia: Geothermics, v. 17, p. 477–488.

Furman, T., 2003, Geochemical overview of the East African rift system: Eos (Transactions, American Geophysical Union), v. 84, no. 46, abs. S52G-03.

Gibson, I.L., 1967, Preliminary account of the volcanic geology of Fantale, Shoa: Addis Ababa: Geophysical Observatory Bulletin, v. 10, p. 59–67.

Hole, J.A., 1992, Nonlinear high-resolution three-dimensional seismic travel time tomography: Journal of Geophysical Research, v. 97, p. 6553–6562.

Horner-Johnson, B.C., Gordon, R.G., Cowles, S.M., and Argus, D.F., 2003, The angular velocity of Nubia relative to Somalia and the location of the Nubia-Somalia-Antarctica triple junction: Eos (Transactions, American Geophysical Union), v. 84, no. 46, abs. T52F-01.

Keller, G.R., Harder, S.H., O'Reilly, B., Mickus, K., Tadesse, K., Maguire, P.K.M., and the EAGLE Working Group, 2004, A preliminary analysis of crustal structure variations along the Ethiopian Rift, *in* Yirgu, G., et al., eds., Proceedings of International Conference on the East African Rift System, June 20–24 2004, Addis Ababa, Ethiopia: Ethiopian Geoscience and Mineral Engineering Association, p. 97–101.

Maguire, P.K.H., Ebinger, C.J., Stuart, G.W., Mackenzie, G.D., Whaler, K.A., Kendall, J.-M., Khan, M.A., Fowler, C.M.R., Klemperer, S.L., Keller, G.R., Harder, S., Furman, T., Mickus, K., Asfaw, L., Ayele, A., and Abebe, B., 2003, Geophysical project in Ethiopia studies continental breakup: Eos (Transactions, American Geophysical Union), v. 84, p. 337, 342–343.

Mahatsente, R., Jentzsch, G., and Jahr, T., 1999, Crustal structure of the Main Ethiopian rift gravity data: 3-dimensional modeling: Tectonophysics, v. 313, p. 363–382.

Menzies, M.A., Klemperer, S.L., Ebinger, C.J., and Baker, J., 2002, Characteristics of volcanic rifted margins, *in* Menzies, M.A., et al., eds., Volcanic rifted margins: Geological Society of America Special Paper 362, p. 1–14.

Montelli, R., Nolet, G., Dahlen, F.A., Masters, G., Engdahl, E.R., and Hung, S., 2004, Finite-frequency tomography reveals a variety of plumes in the mantle: Science, v. 303, p. 338–343.

Parsons, T., and Thompson, G.A., 1993, Does magmatism influence low-angle normal faulting?: Geology, v. 21, p. 247–250.

Pik, R., Deniel, C., Coulon, C., Yirgu, G., and Marty, B., 1999, Isotopic and trace element signatures of Ethiopian flood basalts: Evidence for plume-lithosphere interactions: Geochimica et Cosmochimica Acta, v. 63, p. 2263–2279.

Sinton, J.M., and Detrick, R.S., 1992, Midocean ridge magma chambers: Journal of Geophysical Research, v. 97, p. 197–216.

WoldeGabriel, G., Aronson, J.L., and Walter, R.C., 1990, Geology, geochronology, and rift basin development in the central sector of the Main Ethiopian rift: Geological Society of America Bulletin, v. 102, p. 439–485.

Wolfenden, E., Ebinger, C., Yirgu, G., Deino, A., and Ayalew, D., 2004, Evolution of the northern Main Ethiopian rift: Birth of a triple junction: Earth and Planetary Science Letters, v. 224, p. 213–228.

Manuscript received 14 April 2004
Revised manuscript received 27 July 2004
Manuscript accepted 6 August 2004

Printed in USA

DR2004155

Appendix DR1

Examples of data from shotpoint 26 along 2-D lines are shown in Figure DR-1. Predicted arrival times from the model are overlain on the actual data, which is reduced at 6 km/s. The southern end of the inline shot has a much lower signal-to-noise ratio than other regions of the data, which is true for all shots.

Synthetic seismic models are included in Figures DR-2 through DR-4. The first model, in Figure DR-2, is a simplification of our velocity model of the central region, showing the anomalies below the magmatic segments of Koka, Boseti, and Fantale-Dofan, and the high-velocity anomaly off-axis NW of the Koka segment. The goal of this inversion is to demonstrate that if these features are present, they can be successfully recovered by the inversion. This model was input into the same code using the same sources and receivers as in the actual inversion. As the recovered model indicates, the features are well-recovered and can be successfully imaged.

A non-segmented mafic intrusion is shown in Figure DR-3. This synthetic model was created to test whether the segmentation visible in the actual model (Figure 2) is real or an artifact of poor ray coverage. The intrusion covers the magmatic segments of Boseti and Fantale-Dofan. The recovered model shows that the entire intrusion is recovered with no apparent segmentation, supporting the interpretation that the segmentation is real and corresponds to the segmentation of magmatic segments at the surface.

The final synthetic model is a cross-section along line A-A' (Figure 1). The purpose of the model is to show the amount of lateral smearing of the high-velocity body as well as to test whether 30% diking should be visible in the output model. As can be seen, the main high-Vp body is recovered with only slight lateral smearing, and the dikes are manifested as a continuation of the main anomaly to shallower depths. This would indicate that diking of 30% should be visible in the actual model if present in the magmatic segments, although the diking here is distributed as 6.8 km/s dikes 2-km-wide (due to the limitations imposed by our cell size).

Another method to test whether 30% diking should be evident in our model is to calculate what the bulk velocity effect would be if the dikes were widely distributed in thin sheets throughout the model. Several kilometers beneath the rift axis, the velocity in the recovered model is ~3.8 km/s (Figure 3a). If this is due to a combination of sediments and 30% intruded dikes at 6.8 km/s, one can calculate what sediment velocity is required for a bulk velocity of 3.8 km/s. The calculations result in a required velocity of 2.35 km/s for the sediments if 30% diking is present, which is unlikely. If only 20% diking is present, the required sediment velocity is 2.8 km/s, a more reasonable value. Based on both the synthetics and these rough calculations, we estimate the upper bound on diking throughout the magmatic segments as ~30%.

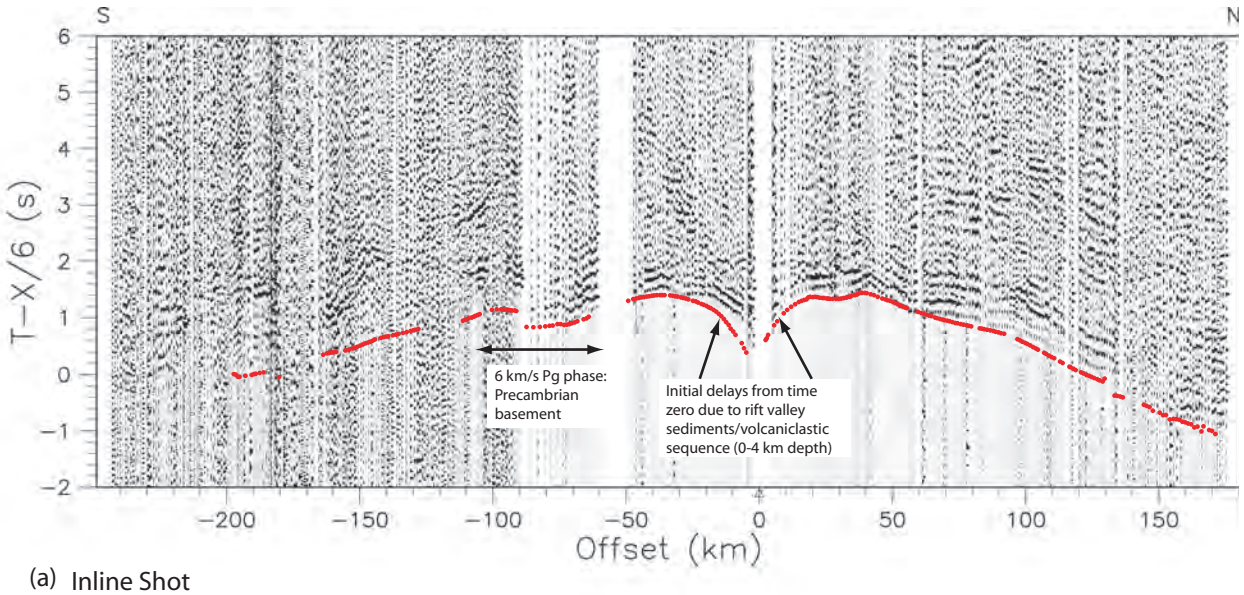

(a) Inline Shot

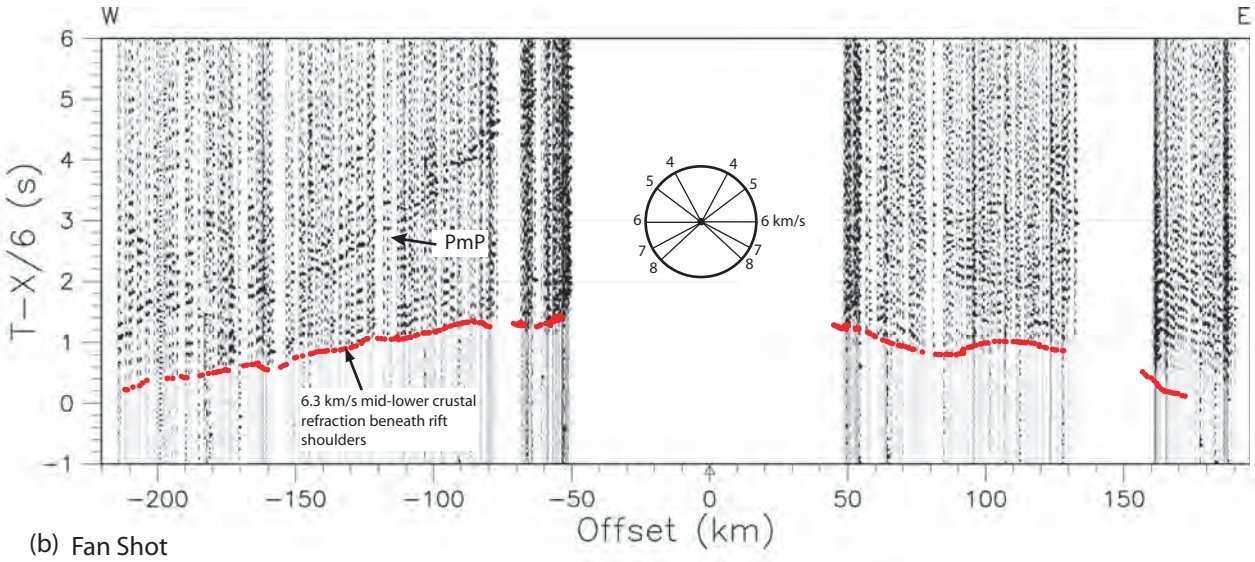

(b) Fan Shot

Figure DR1: Data reduced at 6 km/s from shotpoint 26 into instruments on (a) the along-axis line and (b) the across-axis line. Traces are filtered using a bandpass filter from 2-12 Hz. Note low signal-to-noise ratio on southern end of along-axis line. Predicted travel-times from final model are overlain on traces for an estimate of fit between model and data. RMS deviation of picks for model is ___ ms in (a) and ___ ms in (b). Although short-wavelength features are smoothed slightly, longer wavelength features are very well modeled.

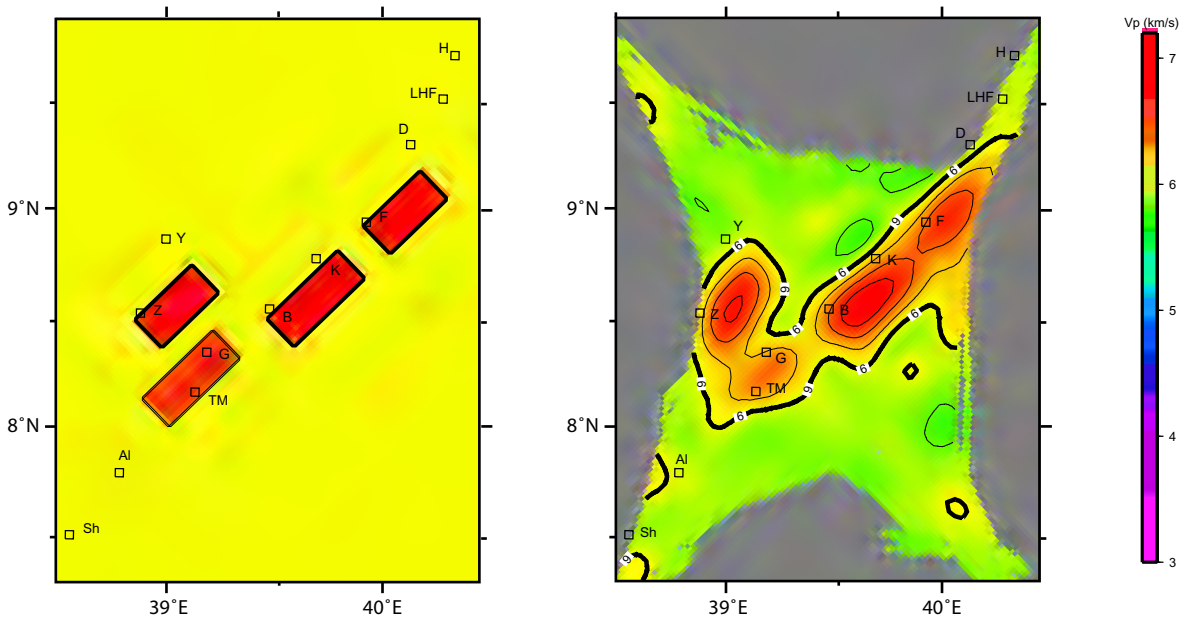

Figure DR2: (a) Synthetic seismic model at a depth of 10 km below the rift floor. Model was input into code used in actual inversion with same sources and receivers to test the ability of the model to recover the interpreted anomalies. Red bodies with high Vp represent mafic intrusions, background velocity is near 6.0 km/s. Locations of volcanoes are shown as diamonds. (b) Output from inversion program. Bodies representing mafic intrusions are well-recovered by the model and segmentation is preserved.

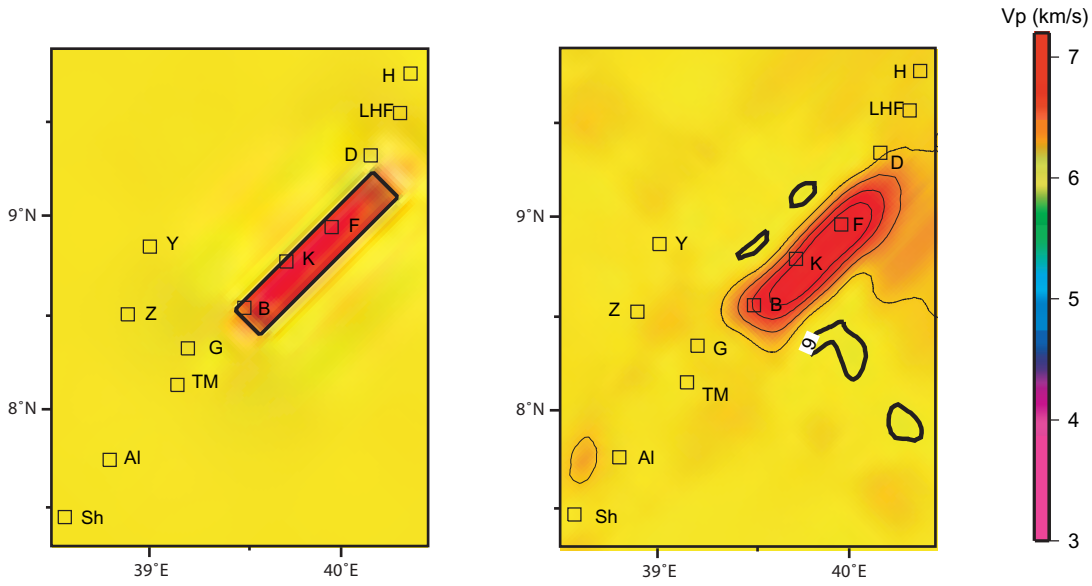

Figure DR3: (a) Synthetic seismic model at a depth of 10 km below the rift floor. Red body represents high-Vp mafic intrusions between the Boseti and Fantale-Dofan segments, but without segmentation. Goal of this model is to test whether ray coverage deficiencies will introduce artificial segmentation into final recovered model. Model was input into code used in actual inversion with same sources and receivers to test the ability of the model to recover the interpreted anomalies. Locations of volcanoes are shown as diamonds. (b) Output from inversion program. Body representing mafic intrusions is well-recovered by the model and no segmentation is introduced.

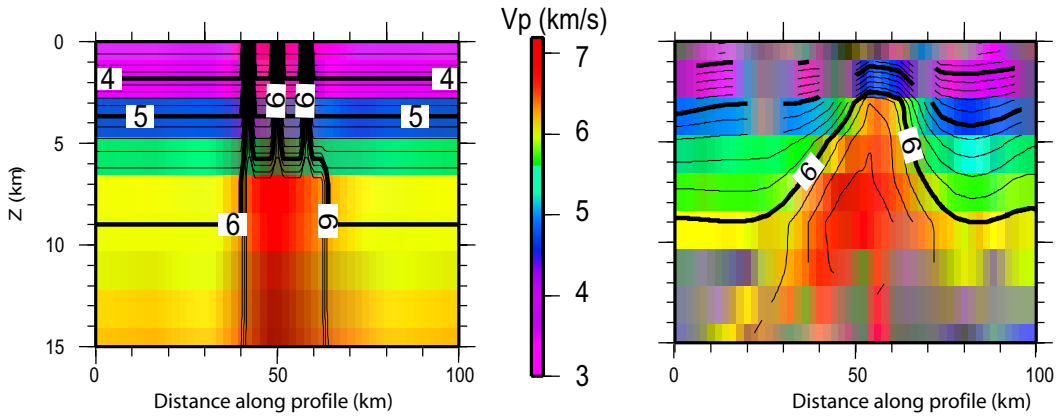

Figure DR4: (a) Synthetic seismic model at a depth of 10 km below the rift floor. This model shows one of the mafic intrusions in cross-section at the location of section A-A′ (Figure 1), with 30% diking above the main intrusion. The goal of this synthetic is two-fold, first to determine if the main intrusion is recovered, and second, to determine if 30% diking would be visible in the recovered model. Model was input into code used in actual inversion with same sources and receivers. (b) Output from inversion program. Body representing mafic intrusion is well-recovered by the model and diking causes high-velocities to extend to shallow depths. If diking was distributed in this manner across the magmatic segments, it would be visible in the recovered model. Also see text of supplementary material for discussion of bulk velocity increases resulting from thin, widely-dispersed dikes.